

Self-sifting of chain plasmons: the complex optics of Au nanoparticle clusters

L. O. Herrmann,¹ V. K. Valev,¹ J. Aizpurua,² and J. J. Baumberg^{1,*}

¹*NanoPhotonics Centre, Cavendish Laboratory, University of Cambridge, JJ Thomson Avenue, Cambridge, CB3 0HE, UK*

²*Material Physics Center CSIC-UPV/EHU and Donostia International Physics Center DIPC, Paseo Manuel de Lardizabal 5, 20018 Donostia-San Sebastian, Spain*

[*jjb12@cam.ac.uk](mailto:jjb12@cam.ac.uk)

Abstract: The strong enhancement of electrical fields in subnanometer gaps of self-assembled gold nanoparticle clusters holds great promise for large scale fabrication of sensitive optical sensing substrates. Due to the large number of involved nanoparticles, however, their optical response is complex and not easily accessible through numerical simulations. Here, we use hyperspectral supercontinuum spectroscopy to demonstrate how confined optical modes of well defined energies are supported by different areas of the cluster. Due to the strong resonant coupling in those regions, the cluster essentially acts as a nanoscale optical sieve which sorts incident light according to its wavelength.

© 2013 Optical Society of America

OCIS codes: (290.5820) Scattering measurements; (240.6680) Surface plasmons; (110.4234) Multispectral and hyperspectral imaging.

References and links

1. I. Hussain, M. Brust, J. Barauskas, and A. I. Cooper, "Controlled step growth of molecularly linked gold nanoparticles: from metallic monomers to dimers to polymeric nanoparticle chains," *Langmuir* **25**, 1934–1939 (2009).
2. M. Grzelczak, J. Vermant, E. M. Furst, and L. M. Liz-Marzán, "Directed self-assembly of nanoparticles," *ACS Nano* **4**, 3591–3605 (2010).
3. J. A. Fan, C. Wu, K. Bao, J. Bao, R. Bardhan, N. J. Halas, V. N. Manoharan, P. Nordlander, G. Shvets, and F. Capasso, "Self-assembled plasmonic nanoparticle clusters," *Science* **328**, 1135–1338 (2010).
4. R. Jin, "Nanoparticle clusters light up in SERS," *Angew. Chem. Int. Edit.* **49**, 2826–2829 (2010).
5. R. W. Taylor, T.-C. Lee, O. A. Scherman, R. Esteban, J. Aizpurua, F. M. Huang, J. J. Baumberg, and S. Mahajan, "Precise subnanometer plasmonic junctions for SERS within gold nanoparticle assemblies using cucurbit[n]uril "glue",*" ACS Nano* **5**, 3878–3887 (2011).
6. S. Kasera, F. Biedermann, J. J. Baumberg, O. A. Scherman, and S. Mahajan, "Quantitative SERS using the sequestration of small molecules inside precise plasmonic nanoconstructs," *Nano Lett.* **12**, 5924–5928 (2012).
7. Á. Sánchez-González, S. Corni and B. Mennucci, "Surface-enhanced fluorescence within a metal nanoparticle array: The role of solvent and plasmon couplings," *J. Phys. Chem. C* **115**, 5450–5460 (2011).
8. A. M. Schwartzberg, C. D. Grant, A. Wolcott, C. E. Talley, T. R. Huser, R. Bogomolni, and J. Z. Zhang, "Unique gold nanoparticle aggregates as a highly active surface-enhanced Raman scattering substrate," *J. Phys. Chem. B* **108**, 19191–19197 (2004).
9. L. Polavarapu and Q. H. Xu, "Water-soluble conjugated polymer-induced self-assembly of gold nanoparticles and its application to SERS," *Langmuir* **24**, 10608–10611 (2008).
10. M. C. Daniel and D. Astruc, "Gold nanoparticles: assembly, supramolecular chemistry, quantum-size-related properties, and applications toward biology, catalysis, and nanotechnology," *Chem. Rev.* **104**, 293–346 (2004).
11. B. Yan, A. Thubagere, W. R. Premasiri, L. D. Ziegler, L. Dal Negro, and B. M. Reinhard, "Engineered SERS substrates with multiscale signal enhancement: nanoparticle cluster arrays," *ACS Nano* **3**, 1190–202 (2009).

12. F. L. Yap, P. Thoniyot, S. Krishnan, and S. Krishnamoorthy, "Nanoparticle cluster arrays for high-performance SERS through directed self-assembly on flat substrates and on optical fibers," *ACS Nano* **6**, 2056–2070 (2012).
13. I. Blakey, Z. Merican, and K. J. Thurecht, "A method for controlling the aggregation of gold nanoparticles: tuning of optical and spectroscopic properties," *Langmuir* **29**, 8266–8274 (2013).
14. T. A. Laurence, G. Braun, C. Talley, A. Schwartzberg, M. Moskovits, N. Reich, and T. Huser, "Rapid, solution-based characterization of optimized SERS nanoparticle substrates," *J. Am. Chem. Soc.* **131**, 162–169 (2009).
15. B. Yan, S. V. Boriskina, and B. M. Reinhard, "Optimizing gold nanoparticle cluster configurations ($n \leq 7$) for array applications," *J. Phys. Chem. C* **115**, 4578–4583 (2011).
16. M. Quinten and U. Kreibig, "Optical properties of aggregates of small metal particles," *Surf. Sci.* **172**, 557–577 (1986).
17. K. Kelly, E. Coronado, L. L. Zhao, and G. C. Schatz, "The optical properties of metal nanoparticles: the influence of size, shape, and dielectric environment," *J. Phys. Chem. B* **107**, 668–677 (2003).
18. V. Myroshnychenko, J. Rodríguez-Fernández, I. Pastoriza-Santos, A. M. Funston, C. Novo, P. Mulvaney, L. M. Liz-Marzán, and F. J. García De Abajo, "Modelling the optical response of gold nanoparticles," *Chem. Soc. Rev.* **37**, 1792–1805 (2008).
19. R. Esteban, R. W. Taylor, J. J. Baumberg, and J. Aizpurua, "How chain plasmons govern the optical response in strongly interacting self-assembled metallic clusters of nanoparticles," *Langmuir* **28**, 8881–90 (2012).
20. L. S. Slaughter, B. A. Willingham, W. S. Chang, M. H. Chester, N. Odgen, and S. Link, "Toward plasmonic polymers," *Nano Lett.* **12**, 3967–3972 (2012).
21. M. Hentschel, M. Schäferling, B. Metzger, and H. Giessen, "Plasmonic diastereomers: adding up chiral centers," *Nano Lett.* **13**, 600–606 (2013).
22. Y. Zhao, L. Xu, and L. M. Liz-Marzán, "Alternating plasmonic nanoparticle heterochains made by polymerase chain reaction and their optical properties," *J. Phys. Chem. Lett.* **4**, 2230–2241 (2013).
23. M. Grzelczak, J. Pérez-Juste, P. Mulvaney, and L. M. Liz-Marzán, "Shape control in gold nanoparticle synthesis," *Chem. Soc. Rev.* **37**, 1783–1791 (2008).
24. P. Alexandridis, "Gold nanoparticle synthesis, morphology control, and stabilization facilitated by functional polymers," *Chem. Eng. Technol.* **34**, 15–28 (2011).
25. C. Ciraci, R. T. Hill, J. J. Mock, Y. Urzhumov, A. I. Fernández-Domínguez, S. A. Maier, J. B. Pendry, A. Chilkoti, and D. R. Smith, "Probing the ultimate limits of plasmonic enhancement," *Science* **337**, 1072–1074 (2012).
26. H. Okamoto, K. Imura, T. Shimada, and M. Kitajima, "Spatial distribution of enhanced optical fields in monolayered assemblies of metal nanoparticles: Effects of interparticle coupling," *J. Photochem. Photobiol. A Chem.* **221**, 154–159 (2011).
27. S. Lin, M. Li, E. Dujardin, C. Girard, and S. Mann, "One-dimensional plasmon coupling by facile self-assembly of gold nanoparticles into branched chain networks," *Adv. Mater.* **17**, 2553–2559 (2005).
28. K. Imura, H. Okamoto, M. K. Hossain, and M. Kitajima, "Visualization of localized intense optical fields in single gold-nanoparticle assemblies and ultrasensitive Raman active sites," *Nano Lett.* **6**, 2173–2176 (2006).
29. W. Chen, A. Kimel, A. Kirilyuk, and T. Rasing, "Apertureless SNOM study on gold nanoparticles: Experiments and simulations," *Phys. Status Solidi B* **247**, 2047–2050 (2010).
30. T. Shimada, K. Imura, H. Okamoto, and M. Kitajima, "Spatial distribution of enhanced optical fields in one-dimensional linear arrays of gold nanoparticles studied by scanning near-field optical microscopy," *Phys. Chem. Chem. Phys.* **15**, 4265–4269 (2013).
31. M. Bosman, V. J. Keast, M. Watanabe, A. I. Maarroof, and M. B. Cortie, "Mapping surface plasmons at the nanometre scale with an electron beam," *Nanotechnology* **18**, 165505 (2007).
32. A. L. Koh, K. Bao, I. Khan, W. E. Smith, G. Kothleitner, P. Nordlander, S. A. Maier, and D. W. McComb, "Electron energy-loss spectroscopy (EELS) of silver nanoparticles and dimers: Influence of beam damage and mapping of dark modes," *ACS Nano* **3**, 3015–3022 (2009).
33. AuNPs were obtained from British Biocell International Ltd. Cucurbit[7]uril was kindly provided by Dr. O. A. Scherman, Melville Laboratory for Polymer Synthesis, Department of Chemistry, University of Cambridge, Cambridge CB2 1EW, UK.
34. A. Mayoral, C. Magen, and M. Jose-Yacamán, "Nanoscale mapping of plasmon resonances of functional multi-branched gold nanoparticles," *Chem. Commun.* **48**, 8667–8669 (2012).
35. S. Bruzzone, M. Malvaldi, G. P. Arrighini, and C. Guidotti, "Theoretical study of electromagnetic scattering by metal nanoparticles," *J. Phys. Chem. B* **109**, 3807–3812 (2005).
36. M. L. Roldán, S. Sanchez-Cortes, J. V. García-Ramos, and C. Domingo, "Cucurbit[8]uril-stabilized charge transfer complexes with diquat driven by pH: a SERS study," *Phys. Chem. Chem. Phys.* **14**, 4935–4941 (2012).
37. N. Hüsken, Institut des Sciences Moléculaires UMR 5255, Université de Bordeaux 1, 16 Avenue Pey Berland, 33607 Pessac, France, and R. W. Taylor, J. C. Taveau, O. Lambert, O. A. Scherman, J. J. Baumberg, and A. Kuhn are preparing a manuscript to be called "Electrokinetic assembly of one-dimensional nanoparticle chains with cucurbit[7]uril controlled sub-nanometer junctions."
38. H. Okamoto, and K. Imura, "Visualizing the optical field structures in metal nanostructures," *J. Phys. Chem. Lett.* **4**, 2230–2241 (2013).
39. G. Colas des Francs, C. Girard, J. Weeber, C. Chicanne, T. David, A. Dereux, and D. Peyrade, "Optical analogy

- to electronic quantum corrals,” *Phys. Rev. Lett.* **86**, 4950-4953 (2001).
40. C. Chicanne, T. David, R. Quidant, J. Weeber, Y. Lacroute, E. Bourillot, A. Dereux, G. Colas des Francs, and C. Girard, “Imaging the local density of states of optical corrals,” *Phys. Rev. Lett.* **88**, 097402 (2002).
 41. E. H. Linfort and E. Wolf, “Diffraction images in systems with an annular aperture,” *Proc. Phys. Soc. B* **66**, 145–149 (1953).
 42. S. T. McCain, R. M. Willett, and D. J. Brady, “Multi-excitation Raman spectroscopy technique for fluorescence rejection,” *Opt. Express* **16**, 10975–10991 (2008).
 43. A. Wei, B. Kim, B. Sadtler, and S. L. Tripp, “Tunable surface-enhanced Raman scattering from large gold nanoparticle arrays,” *ChemPhysChem* **2**, 743–745 (2001).
 44. K. D. Alexander, K. Skinner, S. Zhang, H. Wei, and R. Lopez, “Tunable SERS in gold nanorod dimers through strain control on an elastomeric substrate.” *Nano Lett.* **10**, 4488–4493 (2010).
-

1. Introduction

Self-assembly of gold nanoparticles (AuNPs) using molecular linkers is a cost-effective, reliable and scalable fabrication method of plasmonic aggregates with subnanometer interparticle separations [1–4]. The large enhancement of electric fields in the gaps between the constituent nanoparticles combined with their ability to assemble *in situ* renders them versatile building blocks for sensing devices exploiting surface-enhanced spectroscopy (SERS, SEIRA, SEF) [5–10]. However, the enhancement of molecular signals sensitively depends on the strength of the local electric fields and the distribution and magnitude of those fields within the clusters therefore greatly affect sensing performance [11–13]. Hence, a precise understanding of the optical coupling of light into self-assembled plasmonic structures is of paramount importance for the optimization of such sensing devices [14, 15].

The optical response of an AuNP aggregate is essentially determined by five parameters: The shape of the constituent particles, their size, the separation between those particles, the refractive index of the surrounding medium and the morphology of the cluster [16–22]. Wet-chemical methods allow the first four parameters to be adjusted reliably [10, 23–25], but it is the inherently random nature of the aggregation process which renders control over the morphology of the aggregates challenging. Unfortunately, the influence of structural changes on the optical response is also the most difficult parameter to assess theoretically. This is due to the large number of possible nanoparticle arrangements and the high computational effort required to calculate their electrodynamic behavior because of the extremely small gaps which are much smaller than the nanoparticle diameters. Remarkably, initial theoretical studies of aggregates containing up to 100 AuNPs suggest that the overall optical response of such clusters is relatively robust under structural deformations [19, 26]. This is understood to be due to selective excitation of plasmons along one-dimensional nanoparticle chains extending through the cluster. The resonance energy of these so called *chain plasmons* is relatively insensitive to disorder within the chain and only weakly affected by nanoparticle chains branching off sideways [5, 27]. The energy of these resonances is therefore expected to be related to the length of the nanoparticle chains within the cluster and their orientation relative to the polarization direction of the incident light. Consequently, we expect a confinement of longer wavelengths modes along extended nanoparticle chains which are predominantly found in the core of the cluster. Conversely, shorter wavelength modes are expected to occur wherever small chains and single particles extrude from the cluster.

To probe this behavior experimentally, we investigate the hyperspectral scattering response of self-assembled nanoparticle clusters with near-uniform interparticle separation using scanning supercontinuum spectroscopy. This reveals information about the spatial distribution of the optical modes within the cluster in the visible and near-infrared regions (500-1000 nm). Previous studies have employed scanning near field optical microscopy (SNOM) [28–30] and electron energy loss spectroscopy (EELS) [31, 32, 34] to probe the near-field distribution around single AuNPs as well as small aggregates. These techniques give rise to very high spatial res-

olution (< 10 nm) and reveal intricate details about the local field distributions, but are slower and more intrusive than far-field optical mapping, and in general cannot access a large spatial area. In particular, the close proximity of the SNOM aperture to the nanostructure may alter the plasmon resonances and therefore affects the measured response [35]. The high energy electron beam required for EELS increases the mobility of surface atoms which tend to fuse nanometric gaps within the aggregates [32], thereby severely affecting their optical properties. In addition, electron spectroscopy is limited to vacuum and can not be used to probe the influence of different immersion liquids. It also picks up the very many dark modes in such aggregates, which are inaccessible in the far field, and thus not directly relevant. Despite the significantly lower spatial resolution of scanning supercontinuum spectroscopy (~ 250 nm), we show that its non-invasive nature and ease of use make it a suited technique to investigate the distribution of radiative localized chain plasmons in self-assembled nanostructures.

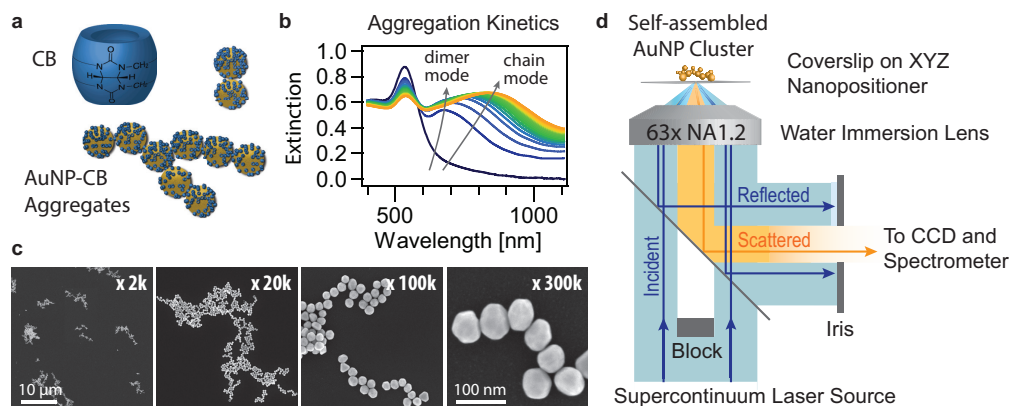


Fig. 1. a) Schematic of gold nanoparticle self-assembly into clusters using the macrocyclic molecule cucurbit[7]uril (CB) as rigid linker. b) Extinction spectra of the first four minutes of the aggregation process. c) Electron microscopy images of the clusters at different magnifications show the cluster and particle morphologies and the uniformity of interparticle separations. d) Supercontinuum laser dark-field spectroscopic setup for rapid collection of full scattering spectra from a diffraction limited spot during sample scanning.

2. Methods

AuNP aggregates were assembled using the macrocyclic molecule cucurbit[7]uril (CB[7], Fig. 1(a)) which is known to yield rigid and reproducible gap sizes of ~ 1 nm [5]. Upon addition of $10 \mu\text{M}$ CB[7] to a 43 pM suspension of 60 nm diameter AuNPs [33], the AuNPs undergo aggregation and quickly form nanoparticle clusters with chain-like sub-units. Their desirable applicability for SERS sensing has been demonstrated previously [5, 6, 36]. The aggregation process is monitored with time-resolved extinction spectroscopy [Fig. 1(b)]. A few seconds after addition of CB[7], a new extinction peak emerges at around 700 nm indicating the formation of dimers. Over time, the formation of longer particle chains and eventually larger clusters cause a red-shift and strong broadening of this peak. After 4 minutes , $50 \mu\text{L}$ of the suspension is drop cast onto an ITO-coated coverslip. We have previously shown using 3D tomographic electron microscopy [37] that gently drop casting such aggregates does not dramatically change their 3D structure, or their plasmonic resonances. Although 2D imaging is used here, our previously reported simulations show little difference between 2D and 3D aggregate plasmonic modes [19], due to the essentially linear dendritic form of the NP connectivity. A Zeiss 1540XB

CrossBeam workstation is used to record scanning electron microscopy images of these clusters [Fig. 1(c)] and to tag them with a focused ion beam mark to aid subsequent localization with an optical microscope.

The hyperspectral scattering response of these clusters is then measured with a total internal reflection microscopy setup exploiting a supercontinuum laser (Fianium SC450-6, 450-1700 nm) as illumination source [Fig. 1(d)]. The inner part of the laser beam is blocked such that the remaining annular beam propagating through the outer part of a water immersion lens (Leica HCX PL APO, NA 1.2) undergoes total internal reflection at the top surface of the sample coverslip. The evanescent wave then excites localized plasmons within the clusters. The emerging scattered light is confocally collected through the inner part of the objective lens (NA 0.9) and sent to a spectrometer while the reflected light is blocked by a complementary iris diaphragm. It is the large spatial coherence of the laser beam which allows confinement of the illumination to a near-diffraction limited spot in the focal plane. The resultant large radiant flux densities enable collection of broadband scattering spectra on a millisecond timescale. In addition, the tight confinement of the illumination gives rise to high lateral spatial resolution (220 nm at $\lambda = 550$ nm, cf. Fig. 4(b)).

A spatial map of the scattering response of a nanoparticle cluster was acquired through step-wise scanning of the sample underneath the focal spot of the laser. For that purpose, the coverslip was rigidly attached to an XYZ nanopositioner (Physik Instrumente P-733.2 and Smaract SLC-2430-S) and scanned in discrete steps over a 2D grid with a step size of 100 nm. A full scattering spectrum was collected at each grid position. The overall acquisition time was limited by the speed of the closed-loop controlled movement of the piezo stage. This resulted in typical scan rates of 10 points per second while recording full scattering spectra at each grid point. For example, a hyperspectral scan of a $5\ \mu\text{m} \times 5\ \mu\text{m}$ area containing 2500 scattering spectra could be acquired in approximately 4 minutes. The position of optimal focus was determined through collection of several scans at different z-positions. While an improvement in acquisition speed could be achieved through scanning of the beam instead of the sample, maintaining achromaticity in the focal spot was found to be challenging.

The robustness of the observed hyperspectral cluster response was confirmed through collection of multiple scans under varying illumination conditions. This was achieved by changing the aperture diameter of the input and output beam, respectively. Furthermore, clusters with different structure were investigated to verify the consistency of the observations.

3. Results and discussion

The measured hyperspectral response of a cluster forms a four-dimensional data cube (x, y, λ, I) where x and y are the spatial positions, λ the wavelength and I the measured scattering intensity. This data is visualized by plotting the scattering intensity as a function of position for multiple discrete wavelengths [Fig. 2(a)]. To aid comparison between different scans, the intensity maps were bi-linearly interpolated and false-colored. Each of these intensity maps reflects the spatial distribution of the normalized scattering response within the cluster at the specified wavelength. An intense response indicates the presence of a radiative localized plasmon mode coupling resonantly to incident light of the given wavelength. Consequently, the local electric field is strongly enhanced at this position. The spatial map therefore reveals information about the uniformity, reproducibility and distribution of the plasmonic surface enhancement across the cluster which is responsible for the signals of field-enhanced spectroscopic techniques such as SERS or SEIRA.

Previously published numerical simulations of the spatial field distribution in such two-dimensional nanoparticle clusters with uniform nanometer interparticle separations have shown the strong localization of short wavelength modes in the peripheral region of the aggregate [19].

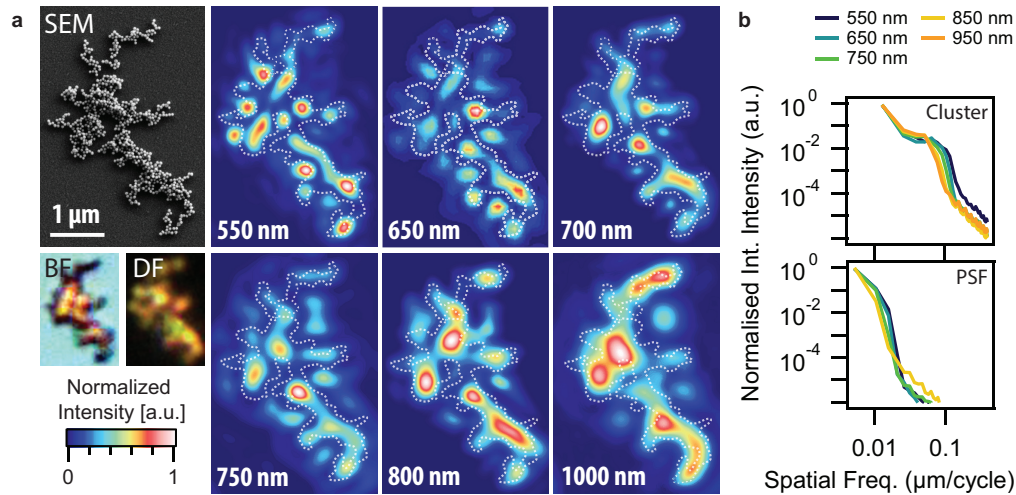


Fig. 2. Scattering response of a self-assembled gold nanoparticle cluster. a) Scanning electron microscope (SEM) image of the cluster together with optical bright-field (BF) and dark-field (DF) images (left). The spatial distribution of the scattering response of the cluster at different wavelengths (right). (Note: Each image shows the same field of view and the light is unpolarized, wavelengths are labeled at the bottom of each image, the gray dotted lines represent the outline of the cluster as extracted from the SEM image). b) Radially averaged and normalized power spectral density of hyperspectral intensity maps (top) and of measured PSF (bottom).

The calculations predicted that with decreasing energy (increasing wavelength) of the excitation field, long chain modes within the core of the aggregate begin to dominate the optical response. The intensity maps in Fig. 2 indeed confirm this position selective excitation of short and long chain modes which do not simply scale with the wavelength of the light [Fig. 2(b)]. At higher energies (550-650 nm), single particle and dimer modes dominate the response. They are mainly located in the periphery of the cluster. The near isotropic interlinkage between nanoparticles in the core of the aggregate prevents the excitation of higher energy modes transverse to the direction of extended nanoparticle chains. For example, it is clearly visible that wherever the cluster is nearly close-packed, the scattering response between 550-650 nm vanishes almost entirely. On the other hand in the periphery, dimers and short chains branch off from the main cluster in perpendicular directions and their resonances can therefore be selectively excited with light polarized along those directions. At longer wavelengths around 800 nm, the cluster modes start to successively concentrate along the longer chains in the denser parts of the aggregate, since only these extended resonant structures can support such low energy modes. At around 1000 nm, the spatial response spreads along almost the entire core of the aggregate. However, the weak scattering in the central part clearly exposes the poor plasmonic coupling between the lower and the upper part of the aggregate, a feature hardly visible from the SEM images.

The relatively dominant wavelength of the plasmons at each position is plotted in Fig. 3(a) for three different clusters. Each scan was normalized at each wavelength to account for the different scattering efficiency of the various chain modes. The pixel of the intensity maps were then colored according to the wavelength position of the normalized scattering maximum. This reveals how short chain modes are squeezed out towards the periphery whereas longer wavelength modes dominate the response in the center of the cluster. The cluster therefore sifts the incident light and confines it to chain plasmons in accordance to its wavelength [Fig. 3(b)]. The

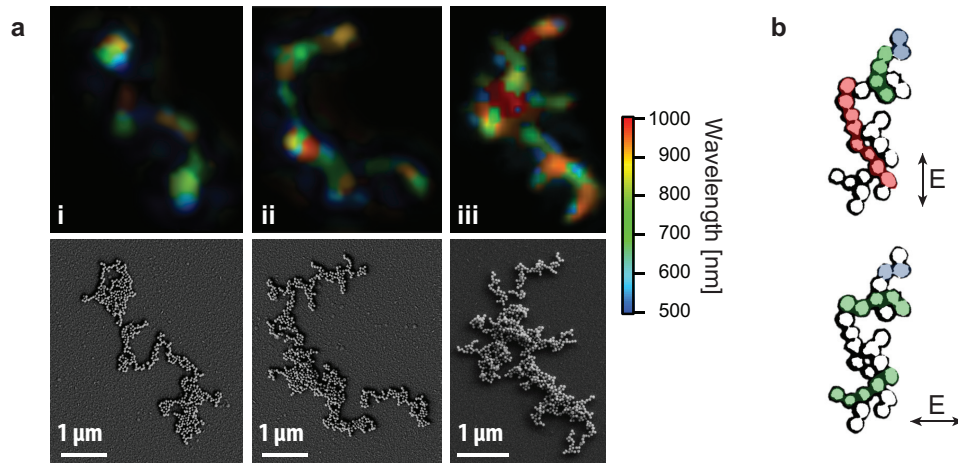


Fig. 3. a) False color image showing the wavelength of the dominant mode at each spatial position (top) together with the corresponding SEM images of the cluster (bottom). b) Schematic of a small cluster illustrating the excitation of various chain plasmons with differing resonant wavelengths (blue = short, red = long) for vertically and horizontally polarized light.

resulting plasmon mode distribution is determined by the underlying topological arrangement of the nanoparticles and is in general highly non-uniform. Consequently, the efficiency of the local field enhancement varies with the position of the analyte within the cluster. Such a cluster can therefore be used as a position selective sensing substrate with sub-diffraction spatial resolution.

Clusters with different structure were investigated to verify the consistency of the observations. The described trends were clearly visible in all fractal-like dendritic clusters, but were less pronounced in the grape-like, dense clusters obtained in reaction-limited aggregation processes (using lower CB[7] concentrations). This is expected due to the reduced number of exposed particle chains in those clusters and the absence of short nanoparticle chains in the peripheral regions. Indeed, it has been reported previously that such dense clusters preferentially localize the electric field in the peripheral regions [38].

The intensity maps also show the presence of weaker ‘ghost’ modes in the close vicinity of the aggregate. These additional modes become more discernible in a logarithmic plot of the integrated scattering response of the cluster [Fig. 4(a)]. The intense scattering from the body of the cluster (false-colored in blue) is surrounded by a weaker scattering band (red) which is separated from the central part by a darker ring. This additional scattering could originate from electromagnetic fields in the vicinity of the surface which radiatively couple to the far-field [39, 40]. However, most of those localized states outside the aggregate are non-radiative and we believe that the observed additional modes are more likely an artifact due to the convolution of the scatterer with the point spread function (PSF) of the system. The accurate response is further complicated through the varying plasmonic enhancement of the scattering in the area of overlap between the cluster and the higher order Airy rings of the illumination. A simple deconvolution can therefore not fully eliminate those ghost modes.

To determine the PSF, a gold nanorod (AuNR, 10 nm x 40 nm) was scanned underneath the focal spot of the laser [Fig. 4(b)]. An AuNR supports two non-degenerate plasmon modes, a longer wavelength (lower energy) mode originating from electron oscillations along its longitudinal axis and a shorter wavelength (higher energy) mode from oscillations in the transverse

direction. Due to its small dimensions, the AuNR effectively acts as a point source. Its resonant scattering at 550 nm (transverse mode) and 800 nm (longitudinal mode for a rod with a length/width ratio of ~ 4) allows extraction of the PSF in the range between 550-900 nm. The shape of the PSF can be adequately described by scalar diffraction theory. This predicts that a plane wave passing through the circular back aperture of an objective forms an Airy pattern in the focal plane which carries $\sim 80\%$ of the energy in its central lobe [41]. With increasing annular obstruction of the back aperture, more energy is shifted into the outer rings of the Airy disk. For the obstruction ratio used here ($\epsilon = 0.5$ where ϵ is the ratio of obstruction radius to aperture radius), only $\sim 50\%$ of the light passes through the central lobe of the Airy disk. At the same time, the linear obstruction increases the lateral confinement of the beam leading to slightly enhanced spatial resolution. When the laser is focused in the immediate vicinity of the cluster, the outer rings of the Airy pattern still overlap with the nanoparticle aggregate and are able to excite plasmon modes in the cluster. The extent and resonant structure of the area where this overlap occurs then essentially determines the strength of the ghost mode outside the aggregate. Since the diffraction pattern of an aperture scales linearly with wavelength, the FWHM of the PSF increases proportional to the wavelength. Thus, the separation of the ghost mode from the aggregate depends on its resonant color.

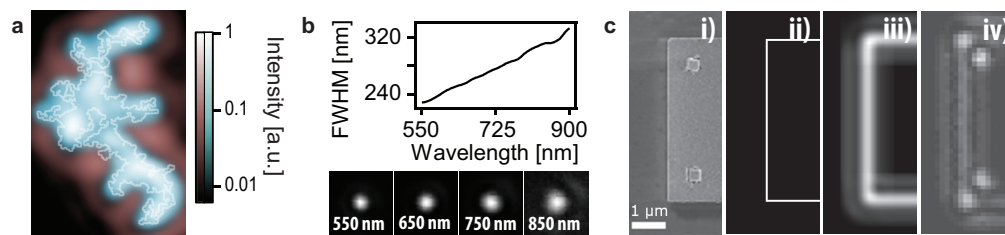


Fig. 4. a) Logarithmic intensity map of the total scattering response of the cluster in Fig. 2 between 500 and 1000 nm. The primary scattering from the cluster is false-colored in blue, the surrounding 'ghost' modes in red. b) (Top) Spatial resolution of setup: Wavelength dependence of FWHM of measured point spread function (PSF). (Bottom) Measured PSF. c) Investigation of the scattering from the edge of a gold rectangle on a silicon substrate (i). Convolution of the PSF of the system (at 800 nm) with a sub-diffraction line (ii) produces the theoretically predicted scattering map (iii). This is in reasonable agreement with the measured scattering map, but does not reproduce the hot-spots in the edges (iv).

To further investigate the origin of these ghost modes, we investigated the scattering from the edge of a gold rectangle ($5\ \mu\text{m} \times 5\ \mu\text{m} \times 15\ \text{nm}$) on a silicon substrate [Fig. 4(c)]. In each corner of this rectangle, there are smaller rectangles ($250\ \text{nm} \times 250\ \text{nm} \times 15\ \text{nm}$) which aid in focusing the sample. The edge of the large rectangle acts as a sub-diffraction scatterer. The convolution of the PSF of our imaging system with a thin line representing the scattering edge of the rectangle (ii) therefore produces the theoretically predicted image of this structure (iii). The obtained image is in reasonable agreement with the measured scattering intensity (iv) and in particular reproduces the secondary intensity bands surrounding the primary scattering from the edge. This substantiates that these bands originate from the overlap of the outer rings of the Airy disk with the scatterer. However, the convolution does not reproduce the plasmon enhanced field in the corners of the rectangle which exemplifies why a simple deconvolution of the intensity maps with the PSF cannot be applied.

An alternative approach which confirms that the observed spatial intensity distributions of our aggregates are not purely a diffraction phenomena is to compare the radially averaged and normalized power spectral density (PSD) of the intensity maps to the PSD of the measured point spread function [Fig. 2(b)]. It is evident that the intensity maps carry completely different

frequency components which do not simply scale with the point spread function of the system.

4. Conclusion

In conclusion, we have shown experimentally that self-assembled gold nanoparticle clusters support strongly localized plasmon modes whose resonant energy sensitively depends on their position within the aggregate. Shorter wavelength modes are found in the periphery of the cluster while longer wavelength modes predominantly stretch along extended nanoparticle chains typically found in the core of the aggregate. Even in relatively dense areas of the nanoparticle aggregates, the scattering response is still highly non-uniform which exposes the selective coupling of extended nanoparticle chains to incident light. These observations verify theoretical predictions and confirm that numerical models are a suitable tool to predict the optical behavior of physical aggregates, despite incomplete knowledge about the local dielectric environment and the distribution of gap sizes.

We believe that such hyperspectral measurements combined with theoretical simulations are an extremely useful tool for the optimization of surface enhanced sensors, as they help to understand and improve the energy transfer of excitation lasers into the electric near-field in the gaps between the nanoparticles. The efficiency of this transfer directly influences the signal enhancement (SERS, SEIRA, SEF) and is key to improve sensitivity and response times of nanoparticle sensors. In addition, knowledge of the spatial extent of the modes is of particular importance for the development of multi-excitation and tunable sensing substrates for which a uniform response over an extended spectral range is desirable [42–44].

Acknowledgments

The authors acknowledge funding from UK EPSRC grants EP/H028757/1, EP/H007024/1, EP/G060649/1, ERC 320503 LINASS and EU CUBIHOLES for this work. We also thank Alejandro V. Silhanek for the fabrication of the rectangular gold structures.